A Dual Frequency, Multi-Year Monitoring Program of Compact Radio Sources

T. Joseph W. Lazio, E. B. Waltman

Code 7213, Remote Sensing Division, Naval Research Laboratory, Washington, DC 20375-5351

lazio@rsd.nrl.navy.mil

ewaltman@rsd.nrl.navy.mil

F. D. Ghigo

National Radio Astronomy Observatory, P.O. Box 2, Green Bank, WV 24944

fghigo@nrao.edu

R. L. Fiedler

Code 7260, Remote Sensing Division, Naval Research Laboratory, Washington, DC 20375-5351

fiedler@sealab.nrl.navy.mil

R. S. Foster[1]

Code 7213, Remote Sensing Division, Naval Research Laboratory, Washington, DC 20375-5351

and

K. J. Johnston

US Naval Observatory, 3450 Massachusetts Ave. NW, Washington, DC 20392-5420

ken@spica.usno.navy.mil

ABSTRACT

We present light curves for 149 sources monitored with the Green Bank Interferometer. The light curves are at two radio frequencies (approximately 2.5 and 8.2 GHz) and range from 3 to 15 yrs in length, covering the interval 1979–1996, and have a typical sampling of one flux density measurement every 2 days. We have used these light curves to conduct various variability analysis (rms flux density variations and autoregressive, integrated, moving average modeling) of these sources. We find suggestive, though not unambiguous evidence, that these sources have a common, broadband mechanism for intrinsic variations, in agreement with previous studies of a subset of these source. We also find that the sources generally display a short-term variability ($\sim$ 10 d) that arises from radio-wave scattering in an extended medium. These conclusions extend those of Fiedler et al. who used a sub-sample of these data. The primary motivation for this monitoring program was the identification of extreme scattering events. In an effort to identify ESEs in a systematic manner, we have taken the wavelet transform of the light curves. We find 15 events in the light curves of 12 sources that we classify as probable ESEs. However,

[1]Present address: Roger S. Foster, Booz-Allen & Hamilton Inc., 8283 Greensboro Drive, McLean, VA 22102-3838 USA

we also find that five ESEs previously identified from these data do not survive our wavelet selection criteria. Future identification of ESEs will probably continue to rely on both visual and systematic methods. Instructions for obtaining the data are also presented.

Subject headings: scattering — surveys — radio continuum: general

1. Introduction

Radio light curves of extragalactic sources can be a powerful probe of both intrinsic and propagation-induced variability of the sources. The typical variability time scale of both intrinsic activity and propagation effects requires that multi-year monitoring programs be conducted. A variety of factors make such multi-year monitoring programs difficult to sustain, but a number have been conducted. Recent examples include Ghosh & Gopal-Krishna (1990); Hughes, Aller, & Aller (1992); Valtaoja et al. (1992); Bondi et al. (1994) and Salgado et al. (1999) (see also §1 of Fiedler et al. 1987b).

With respect to intrinsic activity, previous monitoring programs have suggested, though not entirely unambiguously, that the emission from different classes of sources may be produced by the same mechanism, as would be expected from various unification scenarios. Reasonable agreement is found in comparisons of the predicted light curves from shocked jet models (Marscher & Gear 1985; Hughes, Aller, & Aller 1989a) and observed light curves of various sources (BL Lac, Hughes, Aller, & Aller 1989b; 3C 279 and OT 081, Hughes, Aller, & Aller 1991). In these models, the emission results from a synchrotron-emitting plasma propagating along a diverging jet and subject to one or more shocks. Fiedler et al. (1987b) performed a correlation analysis on light curves of a sample of 36 sources and found that BL Lacs and radio-loud quasars had similar correlation functions, suggesting that similar processes produced the emission in both classes of sources. A structure-function analysis of the total intensity of 51 sources monitored by the University of Michigan Radio Astronomy Observatory (Hughes et al. 1992) also showed that BL Lac objects and radio-loud quasars exhibit similar, power-law structure functions.

However, these comparisons, particularly those of Hughes et al. (1989a) and Hughes et al. (1991), indicated that there are differences in the radio emission process between radio-loud quasars and BL Lacs. Hughes et al. (1992) also found that a structure-function analysis of the Stokes parameters in the frame of reference of the VLBI jet indicated that variations of the polarized flux occur in an orientation related to the underlying jet direction, though with a magnetic field less strongly correlated with jet direction for radio-loud quasars than for BL Lac objects. Flux-based selection effects, due to opacity and Doppler boosting, tend to discriminate against observing the strongest polarization assumed to be present in these categories of sources. Finally, Aller, Aller, & Hughes (1992) concluded that the statistical polarization of 62 Pearson-Readhead sources in the UMRAO monitoring program indicated intrinsic differences between BL Lac objects and radio-loud quasars.

With respect to propagation-induced variability, multi-year monitoring programs of compact sources have shown month- to year-long variations thought to be due to refractive focussing and defocussing of the propagating radiation (Rickett, Coles, & Bourgois 1984). The refractive variations are caused by plasma density fluctuations having typical scale sizes of order an astronomical unit. Propagation-induced variability in a monitoring program can provide information on the angular and/or spatial distribution of these density fluctuations and potentially constrain the microphysics responsible for generating or maintaining these structures. In one case, Bondi et al. (1994) found an annual variation in the scattering properties, which they attributed to changes in the line of sight to sources during the course of the Earth's orbit.

A more extreme example of propagation-induced variability is extreme scattering events (ESE)—a class of dramatic ($\gtrsim 50\%$) decreases in the flux density of extragalactic sources near 1 GHz which persist for weeks to months and are bracketed by substantial increases (Fiedler et al. 1987a). ESEs are infrequent, occurring roughly 1% of the time (Fiedler et al. 1994), so only a multi-year program observing a large number of sources will have a reasonable probability of detecting one.

This paper reports light curves for 149 sources monitored during the interval 1988–1994.4, primarily to search for ESEs. This sample expands upon and includes the 36 sources monitored by Fiedler et al. (1987b, hereinafter Paper I) during the interval 1979–1985. Paper I presented light curves, correlation functions, and structure functions for that 36-source subsample. Light curves for a 46-source subsample monitored during the interval 1979–1987 were presented by Waltman et al. (1991). In addition, interstellar scintillation studies and ESE observations for individual sources were reported by Paper I, Dennison et al. (1987), and Fiedler et al. (1994).

This much larger sample allows us to revisit these issues with a long, densely-sampled monitoring program. In §2 we summarize the observations, in §3 we combine the new observations reported here with those from 1979–1988 and present light curves of the sources and variability analyses employing model light curve functions, structure functions, and wavelet transforms, and in §4 we present our conclusions and instructions for obtaining these data.

2. Observations

The Green Bank Interferometer (GBI) was a facility of the National Science Foundation and was operated by the National Radio Astronomy Observatory under contract with the Naval Research Laboratory (NRL) and the US Naval Observatory (USNO) during the interval 1978 October to 1996 April 1. During the interval 1978–1987, light curves of radio-loud quasars and BL Lacs were obtained during the Earth Rotation Parameters Program operation of the instrument (Paper I; Waltman et al. 1991). During 1988–1994.4 the emphasis of the monitoring program was changed to detect ESEs (Fiedler et al. 1987a), and a program of monitoring compact extragalactic flat-spectrum radio sources for ESEs was instituted. After 1994 the instrument concentrated on Galactic X-ray binaries and extragalactic sources of high-energy radiation. The GBI itself is described by Hogg et al. (1969) and Coe (1973). The observing and calibration procedures relevant to the NRL and USNO observing programs have been described by Paper I and Waltman et al. (1991). Here we shall summarize the details only briefly and call attention to those procedures which have changed since the report of Waltman et al. (1991).

Observations were made on a 2.4 km baseline. Dual circular polarization was recorded over a 35 MHz bandwidth at two frequencies in the S- and X frequency bands. Until 1989 August (1989.7), the frequencies were 2.7 GHz (S-band) and 8.1 GHz (X-band); in 1989 September cryogenic receivers were installed, and the frequencies changed to 2.25 GHz (S-band) and 8.3 GHz (X-band).

Most sources were observed every other day with scans of 10–15 min. integration. Prior to the receiver switch, the observation frequencies were switched between the two frequency bands every 30 s within a scan, and the reported flux densities are daily averages of multiple scans in left-circular polarization only Paper I. The cryogenic receivers both allow the two frequencies to be obtained simultaneously and are more sensitive. After their installation, the observing procedure was changed to acquire typically only a single scan on a source per day. Also, the flux densities reported here for the interval 1988–1994 are the average of left- and right-circular polarizations.

The calibration was ultimately referred to 3C286 (Baars et al. 1977), for which flux densities of 11.85 Jy at 2.25 GHz (10.53 Jy at 2.7 GHz) and 5.27 Jy at 8.3 GHz (5.34 Jy at 8.1 GHz) were assumed. Calibration of the program sources was based on 0237−233 (OD−263), 1245−197 (ON−176.2), 1328+307 (3C286), and 1328+254 (3C287) and was weighted by the difference in time between the observation of the calibration source and the program source. Editing was performed with a running boxcar mean, and data deviating by more than 10σ at X band or 15σ at S band were eliminated.

The uncertainties of the GBI's flux densities measurements are both flux-density and time dependent. (The latter occurring at least in part because of the receiver change in 1989 August.) Paper I presented the following expressions:

$$\begin{aligned} \sigma_S^2 &= (0.037\,\mathrm{Jy})^2 + (0.014 F_S)^2 \\ \sigma_X^2 &= (0.057\,\mathrm{Jy})^2 + (0.049 F_X)^2, \end{aligned} \tag{1}$$

with $F_{S,X}$ the S- and X-band flux densities in Jy. These expressions are appropriate prior to the installation of cryogenic receivers in 1989 August. After the installation of cryogenic receivers, the appropriate expressions are

$$\begin{aligned} \sigma_S^2 &= (0.0037\,\mathrm{Jy})^2 + (0.015 F_S)^2 \\ \sigma_X^2 &= (0.0057\,\mathrm{Jy})^2 + (0.05 F_X)^2. \end{aligned} \tag{2}$$

Because these uncertainties are determined from individual scans, they also represent a measure of the GBI's short-term instrumental stability.

Systematic errors are introduced by atmospheric and hardware effects. By comparing the measured flux densities at various elevation angles with that expected from an average gain curve, we estimate that these systematic errors may approach 10% at S-band and 20% at X-band (occasionally higher for extreme local hour angles). There is also a systematic ripple, with approximately 5% peak-to-peak variations, introduced by the calibration observations of 3C286 (see Figure 8 below). The origin of this ripple is unknown (Paper I), but its 1-yr time scale suggests a seasonally-induced instrumental effect.

3. Light Curves and Analyses (Figure 8)

The list of sources monitored is presented in Table 1, and Figure 1 shows their distribution on the sky in Galactic coordinates. After the expansion of the monitoring program for finding ESEs, sources in or near the Galactic plane were not excluded explicitly. A selection effect against low-latitude sources may remain based on the catalogs used originally to assemble the source list.

Table 1: *Available at http://ese.nrl.navy.mil/GBI/GBI.html*

Most of the columns in Table 1 are self-explanatory. Columns (5) and (6) are the mean flux density over the interval 1989.7–1994. We restrict our attention to this interval because it is the one for which the largest number of sources were present in the monitoring program and to avoid any systematic effects from the change of receivers during 1989. Column (7) is the structure index, which is a measure of how compact the source is on milliarcsecond scales and is defined by Charlot (1990). A source with a structure index of 1 is relatively compact, having 90% or more of its flux density in a single component, while a structure index of 4 indicates a relatively extended source, typically having two or more components of approximately

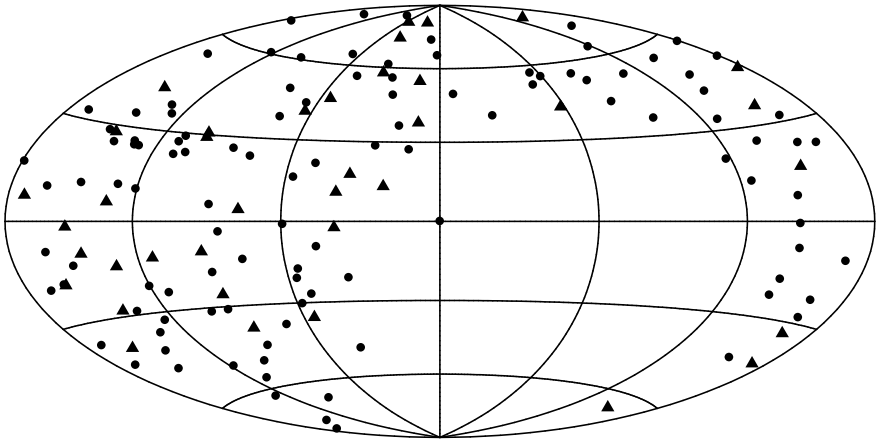

Fig. 1.— The distribution on the sky of sources monitored. Sources observed during the interval 1988–1996 are denoted by triangles; sources whose observations commenced prior to 1988 are denoted by circles. Sources are plotted using their Galactic coordinates, and the Galactic center is at the center of the plot with Galactic longitude increasing to the left.

equal flux density. Structure indices are taken from Fey & Charlot (1996) and Fey & Charlot (2000), who determined the structure indices from the contribution of the sources' structures to interferometric group delays in VLBI observations.

A comment regarding both the structure index and the visible magnitude is warranted. It is well known that sources may show structural changes on milliarcsecond scales on time scales of decades. The structure indices are computed from visibility data obtained after the conclusion of the GBI monitoring program. It is plausible that observations obtained contemporaneously with the GBI program would have produced a different structure index. Similarly, many of these sources are known to be variable at visible wavelengths. The magnitudes cited here are the result of a wide variety of observing programs and have been obtained over more than a decade. Both the structure index and m_V should therefore be taken as indicators of a source's structure and brightness, but future observations could certainly produce different values of either quantity.

Figure 8 presents the light curves of the 149 sources observed. While the durations of the light curves are typically 1988–1994, observations of some sources were conducted on a much longer or much shorter duration. Of particular note are the 40 sources for which observations began prior to 1988, typically between 1979 and 1983. Discontinuities in flux levels at 1989.7 result from the change of observing frequency (§2).

For various reasons, some sources observed previously (Paper I; Waltman et al. 1991) were removed from the observing schedule. These sources were 0215+015, 0814+425 (OJ 425), 0823+493, 1226+023 (3C 273), 1345+125 (4C 12.50), and 1748−253. The light curves for three sources observed during this interval are not included in this compilation because they have been published and comprehensive analyses, including comparison with X-ray observations, have been performed in previous work. These sources are 0236+610 (LSI +61303, Ray et al. 1997), GRS 1915+105 (Foster et al. 1996), and 2030+407 (Cyg X-3, Waltman et al. 1994, 1995, 1996; McCollough et al. 1999).

3.1. Root-Mean-Square Variation

As our first measure of the variability of these sources (Paper I), we use the rms flux density variation about the mean, defined in the standard manner as

$$s_F^2 = \frac{1}{N-1}\sum_i [F(t_i) - m_F]^2 \tag{3}$$

for an N-point, discretely-sampled flux density time series $F(t_i)$ having a mean m_F. The rms flux density incorporates variations on all time scales, in particular, it incorporates the instrumental variations described by equation (2) in addition to any intrinsic variations. In order to avoid a bias from the receiver change, rms flux densities (and the means used to calculate them) are determined utilizing only the data from the interval 1989.7–1994, i.e., after the change in receivers and frequencies.

In order to account for the instrumental contribution, we model the rms flux density as being due to at least three terms

$$s_F^2 = s_{\rm GBI,s}^2 + s_{\rm GBI,l}^2 + s_i^2. \tag{4}$$

Here $s_{\rm GBI,s}$ is the short-term instrumental variability (equation 2), $s_{\rm GBI,l}$ accounts for any long-term gain variations or other long-term instrumental effects, and s_i is the intrinsic variability. In what follows we shall analyze $s'_F \equiv \sqrt{s_F^2 - s_{\rm GBI,s}^2}$. Though there does appear to be a long-term instrumental or systematic variation (namely the annual ripple), this variation does not appear to be flux-density dependent and its magnitude is generally smaller than those of the two terms on the right-hand side of equation (4).

Figure 2 shows the rms flux densities from the two frequency bands plotted against each other. Paper I found a high degree of correlation, $r = 0.97$, between the rms flux densities at the two frequency bands. They interpreted this correlation as an indication of a common flaring or variability mechanism in their 36-source sample. Our larger sample displays a similarly high degree of correlation, $r = 0.82$. While our correlation coefficient is numerically lower than that found by Paper I, our larger sample of sources means that the correlation is of higher significance.

The slope of the best-fit line for our sample is 2.14. The variability spectral index ($s_F \propto \nu^\zeta$) is $\zeta = 0.58$ corresponding to an an electron energy density power-law index of 2.5 for the adiabatic stage of a radio flare in the Marscher & Gear (1985) shock model. Analyzing a subset of these sources, Paper I found $\zeta = 0.58$ and an electron density power-law index of 2.4.

Paper I also found that flat-spectrum objects tend to be more variable than steep-spectrum objects. Figure 3 illustrates that this trend continues in our larger sample, though there are more outliers. However, there appears to be no other common property among the steep-spectrum, highly variable sources. For instance, the three most variable sources in Figure 3 with spectral indices $\alpha < -0.5$ are 1308+326 ($\alpha = -0.6$, $s = 49\%$), a relatively compact quasar; 1845+797 ($\alpha = -0.53$, $s = 42\%$), an extended Seyfert 1 galaxy; and 1909+048 ($\alpha = -0.88$, $s = 29\%$), a Galactic X-ray binary.

Because flat-spectrum objects are generally more compact than steep-spectrum objects (Kellermann & Owen 1988), an alternate explanation of, or at least additional contribution to, their variability might be interstellar scintillation. As we discuss below (§3.3), at least a fraction of these sources' variability does arise from interstellar scintillation. Interstellar scintillation will be shown to be important on time scales of order 10 days. However, the rms flux density measures variability on all time scales and tends to be dominated by longer time scale variations, so scintillation is largely unimportant. Figure 4 shows that there is no correlation between a sources's Galactic latitude and its rms flux density; the correlation coefficient between

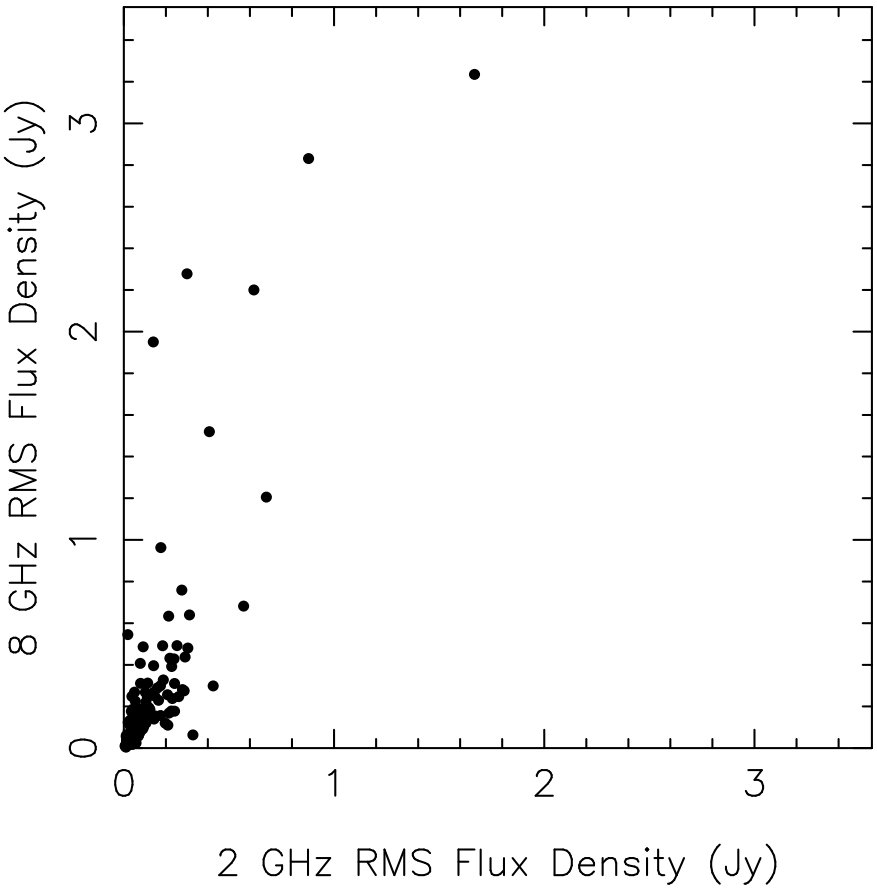

Fig. 2.— The 8.3 GHz rms flux densities plotted against the 2.25 GHz rms flux densities.

rms flux density and Galactic latitude is similar for the two frequencies, $r \simeq -0.05$, and not significant. In any simple model for the contribution of interstellar scintillation to source variability, the contribution should increase for sources closer to the Galactic plane. We regard Figure 4 as an indication that scintillation is not a dominant contribution to the rms variability.

We regard Figures 2 and 3 as evidence of a common flaring or variability mechanism in these sources. First, the 8.3 GHz variability is larger in magnitude than the 2.25 GHz variability. This is consistent with various models in which outbursts or flares are reduced in magnitude (and delayed in time) at low frequencies relative to high frequencies. Second, flat-spectrum sources tend to be more variable than steep-spectrum sources.

While the results of this variability analysis are consistent with the scenario that all sources have a common emission mechanism, we caution that there could be a host of unmodeled systematic effects that could mask true variability or conspire to produce apparent variability. (We regard this as a general difficulty with these kind of analyses, not just with the data from this instrument.) Among the possible systematic effects are elevation and hour angle effects and the sidelobe pattern on the sky. While we see no indications of such effects in these data, others who intend to make use of these data should bear such possibilities in mind.

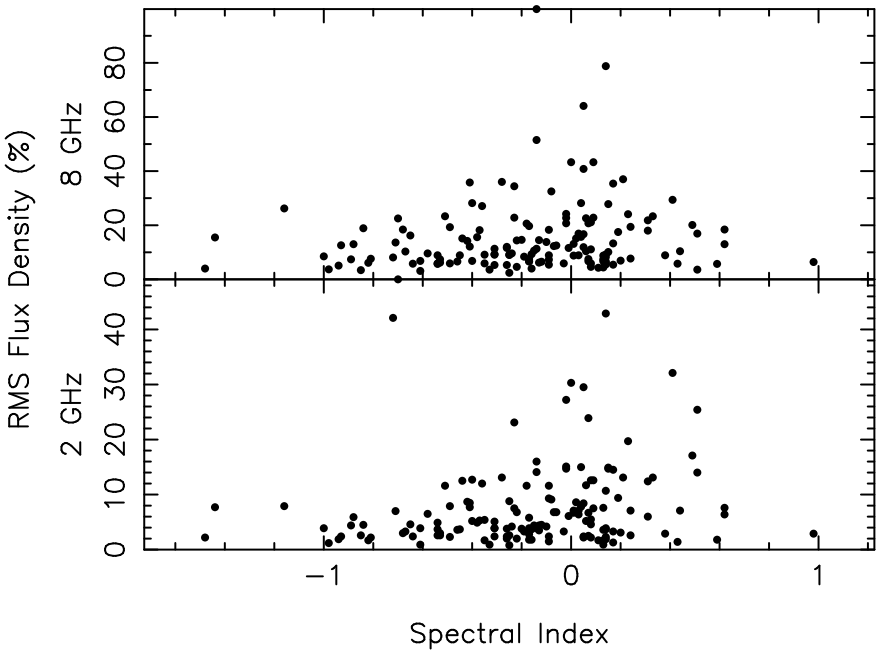

Fig. 3.— RMS flux densities as a function of the median spectral index. *Top*: 8.3 GHz; *Bottom*: 2.25 GHz.

3.2. Light Curve Classification

Paper I conducted an autocorrelation analysis of the light curves presented therein. From the autocorrelation functions (ACFs) they extracted decorrelation time scales. They found strong correlations between the decorrelation time scales at the two frequencies and with the spectral indices of the sources. This ACF analysis in Paper I contributed, in part, to their conclusion that the sources likely had a common emission mechanism.

A key assumption in calculating an ACF is that the underlying time series is in some sense stationary. In extending Paper I's analysis to our larger sample, we have concluded that the assumption of stationarity is not warranted for these light curves and that an ACF analysis can be misleading. One indication that these time series are, in general, not stationary can be obtained from Figure 8. Some of the sources exhibit trends of increasing or decreasing flux density, indicating that that the mean flux density may not be a well-defined quantity and that the time series is not stationary, at least over the length of the time series. We also found that by choosing different sub-intervals of a light curve—for those sources common to this work and Paper I—the qualitative shape and the inferred decorrelation time scale of the ACF could change dramatically, another symptom of non-stationarity.

In their analysis Hughes et al. (1991) employed the first-order structure function to determine the time scale and behavior of their sample of sources, with the time behavior of the sources quantified by means of the logarithmic structure function slope. We defer use of the structure function to §3.3 and employ an alternate means for describing our time series, for two reasons. First, Hughes et al. (1991) find a broad distribution of time scales in their sample. Fully 30% of their sample has a time scale comparable to or longer than the 6-yr duration for which most of this sample has been monitored. A similar structure function analysis of this monitoring program would presumably yield incomplete or biased estimates of the structure function and characteristic time scales. Second, while a relatively simple magnetohydrodynamic model describes the

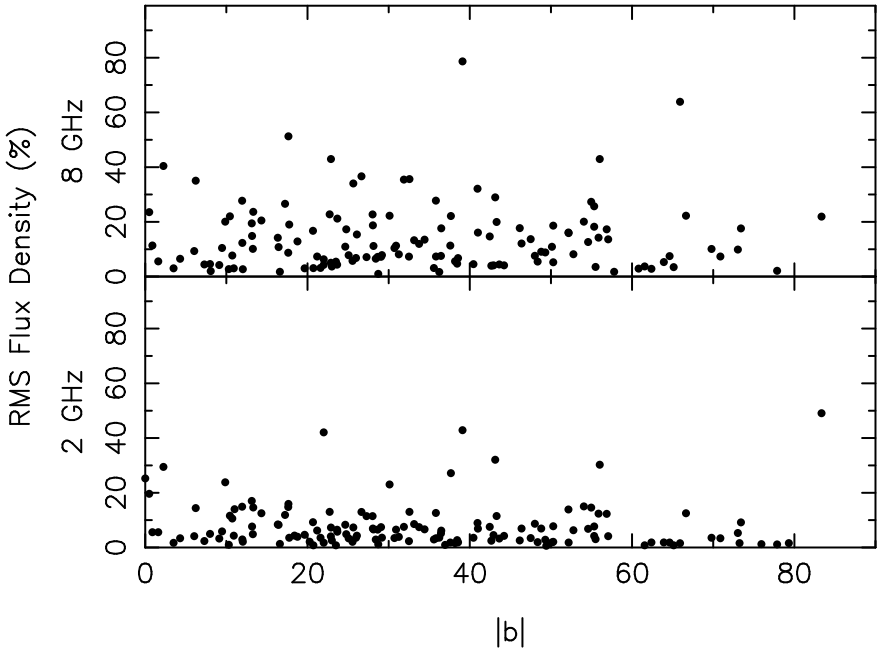

Fig. 4.— RMS flux densities as a function of (absolute) Galactic latitude. *Top*: 8.3 GHz; *Bottom*: 2.25 GHz.

time series of the total and polarized intensity of BL Lac, 3C 279, and OT 081 (Hughes et al. 1989a,b, 1991), there are important differences between the model parameters for the three sources. At least in the context of this class of models, a time series analysis might identify those sources having extreme model parameters or those sources for which the model was not applicable.

As an alternate means of describing these time series, we chose to employ autoregressive, integrated, moving average (ARIMA) models. ARIMA models have found a variety of uses in both describing and forecasting time series for industrial and economic applications (Box et al. 1994) and limited use in astronomy (Scargle 1981; Ögelman 1987; Scargle 1990; Koen & Lombard 1993; Pottschmidt et al. 1998). ARIMA models also have the desirable property that they are not limited to modeling stationary processes.

Our objective is two-fold. First, we assess the extent to which ARIMA models can describe the light curves and to what extent our sample suggests that a common emission process exists for these sources. Second, we wish to identify if there are any sources for which the existing emission models might not be applicable or for which the model parameters might be required to be extreme.

Because of the limited use of ARIMA models in astronomy and for notational purposes, we review the basic ARIMA model. In a p-order AR process the flux value at the current time interval F_i depends upon its values at the p previous time increments and a white noise process f_i:

$$F_i = f_i + \phi_1 F_{i-1} + \phi_2 F_{i-2} + \ldots + \phi_p F_{i-p}, \tag{5}$$

where the ϕ_j are coefficients. In a q-order MA process the flux value at the current time depends upon the values of a white noise process at the current time and q previous time increments

$$F_i = f_i - \theta_1 f_{i-1} - \theta_2 f_{i-2} - \ldots - \theta_q f_{i-q}, \tag{6}$$

where θ_j are coefficients. A d-order integrated process is one in which the value at the current and d previous

time increments is driven by a white noise process

$$F_i + (-1)^1 \binom{d}{1} F_{i-1} + (-1)^2 \binom{d}{2} F_{i-2} + \ldots + (-1)^d F_{i-d} = f_i. \quad (7)$$

Here $\binom{d}{k}$ is the binomial coefficient. A (p, d, q) ARIMA process combines these individual mechanisms. Relevant to the shocked jet flow model (Marscher & Gear 1985; Hughes et al. 1989a) is the white noise process f_i in equations (5), (6), and (7). This white noise process can be considered to be a series of shocks driving the system. An ARIMA process allows the flux density at the current time to depend upon its value and the value of the white noise process at previous times, as might be expected if the emission from these sources arises from multiple, evolving shocks.

We followed analysis procedures described by Box et al. (1994): The various processes can be identified by comparing the behavior of their ACFs and *partial autocorrelation functions*. The partial autocorrelation function measures the correlation between F_i and F_{i-k} taking into account the intermediate values F_{i-1}, F_{i-2}, ..., F_{i-k+1}. Key to our classification of these light curves are the following properties of the ACF and the partial autocorrelation function: For an AR(p) process the ACF cuts off after the first p lags while its partial autocorrelation function tails off exponentially after p lags; conversely, for an MA(q) process the ACF tails off exponentially after q lags while its partial autocorrelation function cuts off after the first q lags. A d-order integrated process can be identified by taking d differences of the time series (equation 7) before forming the ACFs and partial autocorrelation functions. In evaluating whether a partial autocorrelation function or ACF has cut off, we took the fractional uncertainty in estimating both the ACF and partial autocorrelation function to be of order $N^{-1/2}$ for an N-point light curve. In order to minimize any potential effects arising from the receiver switch in 1989, we restricted the analysis to the interval 1989.7–1994.

Earlier we indicated that we found the ACF alone to be an unreliable means of characterizing these light curves. The use of the ACF here does not contradict those earlier statements. First, the difficulty cited with the ACF was due to the non-stationary nature of the light curves. The differencing (equation 7) is designed precisely to reduce the differenced light curve to a stationary, or nearly stationary, time series. Second, the ACF is used here in conjunction with the partial autocorrelation function which is calculated independently and by a different means than the ACF. Thus, even if the ACF is affected by the non-stationarity of the light curve, the partial autocorrelation function will not be.

We have focussed on ARIMA processes with orders p, d, $q \leq 2$. We have imposed this limit for two reasons. First, low-order ARIMA models have had considerable success in describing many other kinds of time series (Box et al. 1994). Second, our focus is on establishing whether a common emission process(es) can describe the light curves. Higher-order ARIMA models may also produce acceptable descriptions of the light curves, though with increasing ARIMA order the reality of the model must be increasingly questioned. Furthermore, if a source cannot be described by any of these low-order ARIMA models that may be an important clue regarding the applicability of the shocked jet model to that source.

Our description of these light curves in terms of ARIMA models is necessarily not unique. First, there is the restriction on the order of the ARIMA models considered, though as noted above high-order ARIMA models may not be realistic. Second, even within our restricted set of models, the solutions may not be unique. For instance, as Box et al. (1994) discuss, the boundary between a stationary and non-stationary process is not distinct. A stationary time series may appear non-stationary if the duration over which it is sampled is too short (and conversely for a non-stationary time series appearing stationary). Finally, there may be other models to describe these light curves besides the class of ARIMA models. Our objective, though, is not to provide a unique description of each light curve, but to assess the extent to which the

different sources may have similar emission mechanisms. For this purpose, the description in terms of ARIMA models is sufficient.

A key assumption in the description (and analysis methods) of ARIMA models is that the time series is sampled uniformly. We do not have uniformly-sampled time series, though they are often nearly uniformly sampled. We have taken two steps to transform these light curves into uniformly sampled time series. First, we have gridded the existing data onto a uniform grid. As the typical spacing between samples is within a few percent of 2 days after 1988, this step should produce little effect on our model identification. Second, we have linearly interpolated between missing data. We have verified in the following manner that this step does not impact adversely our model identification. We took uniformly-sampled time series (series B and C) from the examples provided by Box et al. (1994). We then produced non-uniformly-sampled time series by using the sampling from one of the sources observed, i.e., we introduced gaps whose location and duration were taken from one of the observed light curves. Our model identification procedure nonetheless identified the same models as Box et al. (1994) cite for the uniformly-sampled time series.

Tables 2 and 3 show the model(s) identified for each source at the two frequencies. Table 4 lists those sources for which no model was identified.

Table 2. ARIMA Model Identifications at 2.25 GHz

Source	(1 0 0)	(1 0 1)	(2 0 0)	(2 0 2)	(0 1 1)	(1 1 0)	(1 1 1)	(2 1 0)	(2 1 2)	(0 2 1)	(1 2 1)	(2 2 2)
0003+380				X						X		
0003−066					X		X			X		X
0016+731					X			X		X		
0019+058					X		X			X		X
0035+121										X		X
0035+413								X		X		X
0055+300					X		X					X
0056−001					X		X					
0113−118							X					
0123+257	X	X			X		X			X	X	
0130−171	X	X			X	X	X			X	X	
0133+476					X	X	X			X		X
0134+329					X				X			
0147+187					X		X					
0201+113	X							X		X	X	
0202+319										X		X
0212+735							X					
0224+671					X			X	X	X		X
0235+164					X			X	X	X		X
0237−233					X							X
0256+075					X					X		
0300+470					X	X			X			
0316+413					X				X			X
0319+121					X		X					
0333+321					X					X		
0336−019							X			X		
0337+319					X				X			X
0355+508					X				X	X		X
0400+258							X					
0403−132							X			X		X
0415+379					X			X		X		
0420−014							X			X		X
0440−003					X							
0444+634					X	X			X	X		X
0454+844							X			X		X
0500+019					X		X			X		X
0528+134						X	X					X
0532+826							X			X	X	
0537−158					X			X		X		X
0538+498							X			X		X
0552+398												X
0555−132					X					X		X
0615+820									X			
0624−058					X				X			X
0633+734			X									
0650+371							X			X		X
0653−033					X	X	X			X		X
0716+714									X	X	X	
0723+679		X			X			X	X	X		
0723−008					X					X		X
0742+103			X									
0743+259					X		X			X		X

Table 2—Continued

Source	(1 0 0)	(1 0 1)	(2 0 0)	(2 0 2)	(0 1 1)	(1 1 0)	(1 1 1)	(2 1 0)	(2 1 2)	(0 2 1)	(1 2 1)	(2 2 2)
0759+183		X	X							X	X	
0804+499									X	X		X
0818−128							X			X		X
0827+243										X		X
0837+035		X			X					X		
0851+202							X			X		
0859−140					X					X		X
0922+005					X		X	X		X		X
0923+392					X		X					
0938+119										X		
0945+408					X							
0952+179	X			X			X			X		
1020+400					X				X	X		
1022+194					X		X			X		X
1036−154					X		X			X		X
1038+528							X			X	X	
1055+018										X		
1100+772		X			X						X	
1116+128										X	X	
1123+264					X				X			X
1127−145										X		X
1128+385				X					X	X		
1145−071					X		X			X		
1150+812										X		X
1155+251							X			X		X
1200−051							X			X		X
1243−072	X			X						X		
1245−197			X	X	X				X			X
1250+568		X			X					X		X
1253−055				X								
1302−102					X							
1308+326							X			X		X
1328+307					X				X			X
1354+195										X		
1404+286				X						X		X
1409+524					X				X			
1413+135									X	X	X	
1430−155	X				X		X	X		X		X
1449−012										X		X
1502+106					X					X		X
1511+238					X					X		X
1514+197						X						
1525+314					X	X	X			X		X
1538+149					X	X	X			X		X
1555+001					X		X	X				
1614+051								X				
1624+416					X				X			X
1635−035					X	X	X			X		X
1641+399							X			X		
1655+077					X				X	X		X

Table 2—Continued

Source	(1 0 0)	(1 0 1)	(2 0 0)	(2 0 2)	(0 1 1)	(1 1 0)	(1 1 1)	(2 1 0)	(2 1 2)	(0 2 1)	(1 2 1)	(2 2 2)
1656+477		X	X		X		X	X				X
1741−038					X	X			X	X		
1749+096						X						
1749+701					X		X			X		
1756+237			X		X				X			X
1803+784					X					X		
1807+698									X			
1821+107					X				X	X		X
1823+568	X			X			X			X		X
1828+487					X		X					X
1830+285					X	X			X	X		
1845+797					X		X				X	
1909+048								X	X			
1928+738					X		X			X		X
1943+228					X							X
1947+079												X
2005+403					X				X	X		X
2008−068	X			X	X		X			X		
2032+107					X		X			X		
2037+511					X							X
2047+098												X
2059+034							X	X		X	X	
2105+420					X							
2113+293					X	X	X			X		X
2121+053						X				X		X
2134+004							X			X		X
2155−152					X	X			X			X
2200+420							X					
2209+081					X							X
2214+350										X		X
2251+244					X				X			X
2319+272							X				X	
2344+092					X							X

Note. — Only sources for which at least one ARIMA model was identified are shown, and only ARIMA models that describe at least one source are listed.

Table 3. ARIMA Model Identifications at 8.3 GHz

Source	(1 0 0)	(1 0 1)	(2 0 0)	(2 0 2)	(0 1 1)	(1 1 0)	(1 1 1)	(2 1 0)	(2 1 2)	(0 2 1)	(1 2 1)	(2 2 2)
0003+380									X	X		X
0003−066					X				X			
0016+731					X							
0019+058					X			X	X	X		X
0035+121					X				X			
0055+300					X		X			X		X
0056−001					X		X			X		X
0113−118							X			X		
0123+257	X	X			X		X			X		X
0130−171					X		X	X				
0133+476					X							
0134+329		X			X				X			X
0147+187					X							
0201+113										X		
0202+319									X	X		
0212+735					X				X			
0224+671					X					X		
0235+164								X		X		X
0237−233										X		X
0256+075					X		X					X
0300+470												X
0316+413							X			X		X
0319+121		X					X					
0333+321					X							X
0336−019					X				X			
0337+319		X			X					X		X
0355+508					X					X		X
0400+258										X		
0403−132										X		X
0415+379					X					X		X
0420−014							X			X		X
0440−003									X			
0444+634					X				X	X		X
0454+844					X				X	X		X
0500+019					X				X	X		X
0532+826										X		
0537−158					X					X		
0538+498				X					X	X		X
0552+398									X	X		X
0555−132					X				X			X
0615+820					X					X		
0624−058		X			X				X			X
0633+734					X							
0650+371					X		X					X
0653−033					X				X			X
0716+714					X					X		
0723+679					X				X			
0723−008					X		X					
0742+103		X	X		X				X			X
0743+259					X				X	X		X
0759+183					X				X			X

Table 3—Continued

Source	(1 0 0)	(1 0 1)	(2 0 0)	(2 0 2)	(0 1 1)	(1 1 0)	(1 1 1)	(2 1 0)	(2 1 2)	(0 2 1)	(1 2 1)	(2 2 2)
0804+499					X				X	X		X
0818−128												X
0827+243					X				X			X
0836+710					X				X			X
0837+035					X					X		
0851+202					X				X	X		
0859−140					X				X			
0922+005									X	X		X
0923+392					X				X			
0938+119	X			X								
0945+408									X	X		X
0952+179					X				X			
0954+658										X		
1020+400					X					X		X
1022+194					X				X			
1036−154					X				X			
1038+528					X				X	X		
1055+018					X				X			X
1100+772										X		
1116+128					X				X			X
1123+264										X		X
1127−145					X				X			
1128+385										X	X	
1145−071							X			X		
1150+812					X					X		X
1155+251					X		X			X		X
1200−051					X				X			
1225+368										X		
1243−072					X							X
1245−197					X				X			
1250+568	X				X					X		X
1253−055											X	
1302−102					X		X					X
1308+326									X	X		
1328+307							X			X		
1354+195					X		X					X
1404+286			X		X		X					
1409+524					X							X
1413+135					X				X			
1430−155										X		
1438+385							X			X		X
1449−012					X				X			
1455+247	X			X			X			X		X
1502+106					X							X
1511+238	X									X		X
1514+197							X			X		
1525+314	X			X							X	
1538+149					X				X	X		X
1555+001					X							
1611+343									X	X		X
1614+051					X							

We first assess the relevance of these ARIMA models to the shocked jet models and the analyses described earlier, focussing on BL Lac (2200+420), 3C 279 (1253−055), and OT 081 (1749+096). We shall use only the 8.3 GHz results in this comparison, both because it is a frequency common to the University of Michigan Radio Astronomy monitoring program and this monitoring program and because the 2.25 GHz light curves are affected more strongly by scintillation (§3.3).

Only a single model is identified for both 1253−055 (1,2,1) and 2200+420 (0,1,1). For 1749+096 two models are identified, (1,1,1) and (2,2,2). Hughes et al. (1991) found the opacity within 2200+420 to be less that that of the other two sources. We would therefore expect that the effect of shocks would not persist as long. Hughes et al. (1989a) show this explicitly for a two-shock simulation—in their models, at higher frequencies (lower opacities) shocks are more distinct. Thus, at a given time the observed emission from a low opacity flow is less likely to depend upon its previous values. Exactly that result is observed for the ARIMA models for these three sources. The low order of the 2200+420 model and lack of any MA component to the model indicate that the flux density at any given time is not strongly dependent on its values at previous times.

Like Hughes et al. (1992), we conclude that shocked jet models are widely applicable. A key point regarding Tables 2 and 3 is that most sources can be described by a relatively small number of models. We have constrained p, d, and $q \leq 2$. Thus, for each light curve there are 26 possible models (not counting $p = q = d = 0$) by which it might be described. Yet only 12 models are identified for all sources, and 4 models describe most sources: (0,1,1), (2,1,2), (0,2,1), and (2,2,2). Of these 4 most popular models, (0,1,1) describes 2200+420 and (2,2,2) describes 1749+096 further increasing our confidence in the widespread applicability of shocked jet models.

A similar situation occurs at 2.25 GHz. Only 12 models are identified, and most sources are described by 4 models: (0,1,1), (1,1,1), (0,2,1), and (2,2,2). That nearly the same set of models can identify most sources at both frequencies is an indication that the applicability of the shocked jet model probably extends at least down to 2.25 GHz, even though the effects of interstellar scintillation are also becoming important at this frequency (§3.3).

For most of the sources the light curve can be identified with a $d = 1$ or $d = 2$ model. The use of differencing (eqn. 7) indicates that the light curves are likely to be non-stationary, verifying our earlier statements that many of these light curves appear non-stationary by virtue of not having a well-defined mean.

We have checked whether different classes of sources are over- or under-represented in any model. In general we find no discrepancies between the population of BL Lacs described by each model. Of the total number of sources monitored, 13.4% are BL Lacs. Within the uncertainties, all models describe roughly the same fraction of BL Lacs. Again, like Hughes et al. (1992) we conclude that a similar emission process occurs within both BL Lacs and quasars. That BL Lac objects are identified by a variety of models may indicate other differences within the context of the shocked jet model besides opacity variations as mentioned above, e.g., differences in magnetic field strength or jet viewing angle.

Certain sources often have a large number of models identified for them. These sources are those monitored for the shortest duration and include 0123+257, 0130−171, 1250+568, 1525+314, 1547+508, and 2008−068. The model identification procedure depends upon identifying when an ACF or partial autocorrelation function has effectively dropped to zero. The uncertainty in determining the value of either function at any given lag scales as $N^{-1/2}$. Hence, short-duration light curves are likely to be identified with more than one kind of ARIMA model.

Table 3—Continued

Source	(1 0 0)	(1 0 1)	(2 0 0)	(2 0 2)	(0 1 1)	(1 1 0)	(1 1 1)	(2 1 0)	(2 1 2)	(0 2 1)	(1 2 1)	(2 2 2)
1624+416									X			
1635−035					X				X			
1641+399							X			X		X
1655+077										X		X
1656+477			X	X			X					
1741−038							X					
1749+096							X					X
1749+701										X		
1756+237					X							X
1803+784							X			X		
1807+698					X					X		X
1821+107				X	X				X	X		X
1823+568					X					X		X
1828+487										X		
1830+285					X				X			X
1845+797												X
1909+048								X	X			
1928+738					X					X		X
1943+228					X				X	X		X
1947+079										X		X
2005+403					X				X			X
2008−068								X		X		
2032+107					X					X		X
2037+511										X		
2047+098							X			X		X
2059+034										X		X
2113+293							X					
2121+053					X				X			
2134+004									X	X		
2155−152									X	X		X
2200+420					X							
2214+350					X					X		
2234+282									X	X		X
2251+158					X				X			
2251+244									X	X		X
2319+272					X				X			X
2344+092					X							X
2352+495		X	X		X				X			X

Note. — Only sources for which at least one ARIMA model was identified are shown, and only ARIMA models that describe at least one source are listed.

Two sources deserve special mention because they are *not* quasars or BL Lac objects. The source 1742−289 (Sgr A*) is the compact radio source in the Galactic center. At both frequencies, no model is identified for this source. While 1742−289 is likely to be the radio counterpart to a supermassive black hole, it has also been long recognized that this radio source has a much lower luminosity than those at the cores of active galaxies. The lack of any identified models for 1742−289 is consistent with its emission process being qualitatively different than those of active galaxies.

The source 1909+048 (SS 433) is a microquasar-like source, but the compact object in it is likely to be neutron star rather than a black hole. At both frequencies the models identified for this source are (2,1,0) and (2,1,2). That the model (2,1,2) is a popular model at 8.3 GHz is an indication that certain features of the jet emission from 1909+048 are common to radio-loud quasars and BL Lacs as well.

Finally, we address whether any of the sources for which no ARIMA models are identified (Table 4) are notable in any manner. Of the sources for which a model could not be identified at 8.3 GHz, none of them are BL Lacs, but otherwise there appears to be no other notable aspect. However, examination of their light curves show all of them to be featureless with little indication of variability. These light curves are exactly the kind that would have been excluded by our requirement that p, d, and q could not all be zero, i.e., these light curves are consistent with being dominated purely by white noise. Within the context of the shocked jet model, these sources must be in a period of extended quiescence in which no shocks occur or numerous small shocks occur continually so that the average flux density level remains essentially unchanged.

One potentially puzzling aspect of these identifications is that ARIMA models are identified for 1328+307 but not for 1328+254, even though their light curves are superficially similar. Close examination of the variability measures we have employed for these two sources shows, however, that 1328+307 is slightly more variable; this slight difference is apparent in examination of the levels of the structure functions on long time scales (Figure 9). This additional variability is not due solely to outlier points in the light curves. We have edited out the most visually apparent outliers from the light curve of 1328+307, and it remains more variable than 1328+254. We conclude that the difference in ARIMA models reflects a difference, albeit at a low level, in the variability (i.e., the presence of shocks in the shocked jet model) in these two sources.

We conclude that the sources' emission mechanism(s) is likely to be broadband because the same ARIMA model is identified at both frequencies for most sources. The extent to which the sources have a common emission mechanism is less clear. Only a small number of models is required to describe most sources, but no

Table 4. Sources for which no ARIMA Model Identified

		2.25 GHz		
0836+710	0954+658	1225+368	1328+254	1438+385
1455+247	1611+343	1742−289	2234+282	2251+158
2352+495				
		8.3 GHz		
0035+413	0528+134	1328+254	1742−289	2105+420
2209+081				

model describes more than about 50% of all sources. Only about 20% of the sources are not identified with one of the three most successful models: (0,1,1), (0,2,1), and (2,2,2). We regard this as suggestive evidence that there are a limited number of emission mechanisms that power these sources. It may also be the case that multiple mechanisms are operative in the same source, with differences between sources due to which process is dominant. However, our analysis has not yielded what we regard as unambiguous evidence of a single process powering all sources.

3.3. Structure Functions (Figure 9)

The structure function is useful for removing slow trends in a time series and identifying short time scale fluctuations superposed upon the slow trends. The first-order temporal structure function of the flux density F is

$$D_F(t,\tau) = \langle [F(t) - F(t+\tau)]^2 \rangle \tag{8}$$

(see Simonetti, Cordes, & Heeschen 1985 for a description of higher order structure functions). The first-order structure function removes any linear dependences and reflects the presence of higher-order polynomial terms and stationary processes in the time series, and the slope of the logarithmic structure function is a measure of the temporal structure in the light curve. For a stationary, zero-mean time series with a variance of σ_F^2, the structure function is related to the correlation function $\rho_F(\tau)$ by

$$D_F(\tau) = 2\sigma_F^2[1 - \rho_F(\tau)]^2. \tag{9}$$

As we discuss above (§3.2), the light curves of many of these sources are unlikely to be stationary. For that reason we have employed the definition of the structure function given in equation (8). A "break" in the structure function can be used to identify the characteristic time scale for a process contributing to the time series to saturate (e.g., $\rho[\tau] \rightarrow 0$).

Figure 9 shows the resulting structure functions. Part of the value of the structure function is in identifying short time scale fluctuations. For this reason we have used the *unsmoothed* light curves in forming the structure functions. In constructing these structure functions, we have not used any pairs of data for which one datum was before the receiver change and the other after the receiver change. We also have normalized the structure functions by the variance of the time series. The uncertainties displayed on the structure functions are calculated as (Simonetti et al. 1985)

$$\sigma_D^2(\tau) \approx \frac{8\sigma_F^2}{N_D(\tau)} D_F(\tau) \tag{10}$$

where σ_F^2 is the variance of the time series and $N_D(\tau)$ is the number of data pairs used to form the structure function at lag τ.

Paper I found that, for a subsample of the sources presented here, the typical logarithmic slope of the structure function (calculated using equation [9]) was 1–1.5 for lags less than 20 days. Such a slope is consistent with interstellar scattering resulting from a scattering medium distributed along the line of sight (slope ≈ 1) as opposed to scattering distributed in a screen (slope ≈ 2; Simonetti et al. 1985; Blandford, Narayan, & Romani 1986). Uncorrelated variations would have a logarithmic slope of 0.

We have determined the logarithmic slope for lags ranging between 2 and 32 days. We have used a maximum lag of either 16 or 32 days (i.e., bracketing the maximum lag considered in Paper I) and minimum lags of 2 and 4 days. Because of the day-to-day variability introduced by instrumental effects, the value of the

structure function may contain a contribution from the instrumental variability in addition to any scattering-induced or intrinsic variability. We find that the logarithmic slope for our larger sample is approximately 0.3, with the choice of maximum and minimum lags making little difference. The maximum logarithmic slope for any source is 1.3.

While consistent with a scattering-induced variability on short time scales, the above argument does not rule out an intrinsic contribution to the sources' short-term variability. In an effort to discriminate between an extrinsic and intrinsic origin of the short-term variability, we have compared the structure function slopes to the Galactic latitudes and spectral indices of the sources.

Figure 5 shows the structure function slopes for all sources as a function of (the absolute value of) Galactic latitude, and Figure 6 shows the structure function slopes for all sources as a function of the S/X spectral index. These figures were constructed from the structure function slopes computed using a 2-day minimum lag and 32-day maximum lag. Our expectation is that there should be a latitude dependence if scattering is at least partially responsible for these short-term variations, and a spectral-index dependence if intrinsic variations are at least partially responsible.

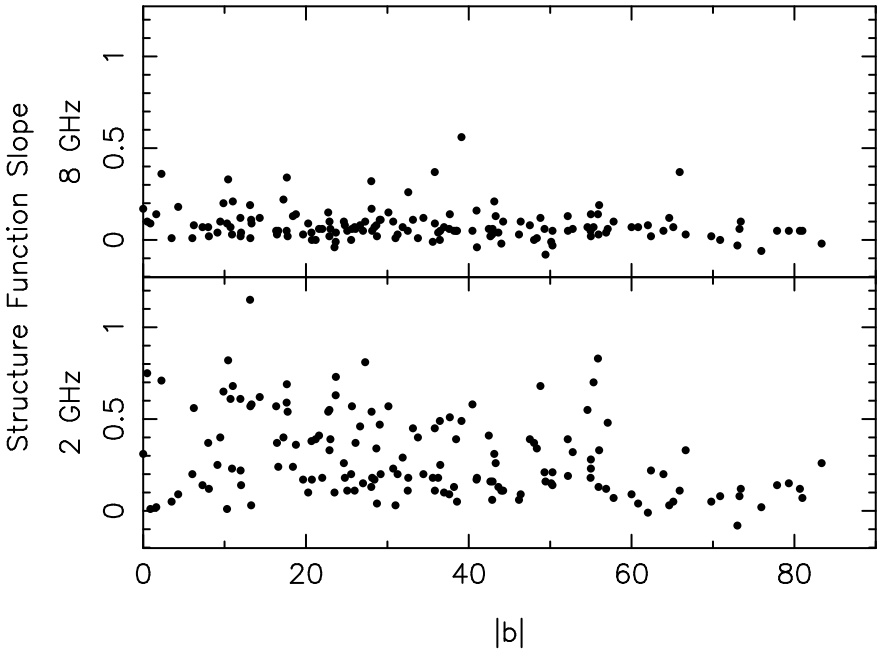

Fig. 5.— Structure function slopes as a function of (absolute) Galactic latitude. Shown are the logarithmic structure function slopes computed for lags between 2 and 32 days. *Top*: X-band (8 GHz); *Bottom*: S-band (2 GHz).

There is a strong correlation between the structure function slopes at 2.25 GHz and Galactic latitude. The correlation coefficient is $r = -0.34$; this strong correlation increases if we bin the data. We can exclude, at better than the 99% confidence level, the hypothesis that the structure function slopes at 2.25 GHz and the sources' Galactic latitudes are uncorrelated. No significant correlation exists between the structure function slopes at 8.3 GHz and Galactic latitude. A strong correlation also exists between the structure function slopes at 2.25 GHz and the S/X spectral index, but not at 8.3 GHz. (We have also verified that there is no correlation between the sources' Galactic latitude and spectral indices which might conspire to produce the

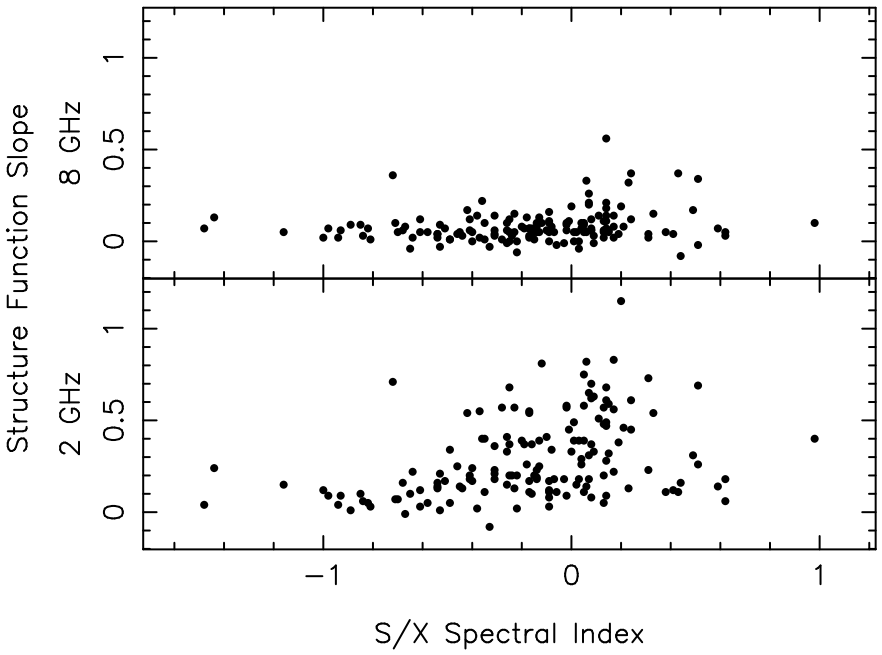

Fig. 6.— Structure function slopes as a function of S/X spectral index. As for Figure 5.

correlations with structure function slopes.)

The strong correlation is essentially unchanged if we remove 1741−038 ($b = 13°$) from the analysis. This source underwent an ESE in 1992, and its inclusion might have been thought to bias the correlation.

We conclude that scattering plays a significant role in causing the short-term ($\sim$ 10 d) variability of these sources or at least those at low latitude. We cannot rule out intrinsic variability also contributing to the short-term variations. If intrinsic variations represent a significant fraction of the short-term variability, however, given that flat-spectrum sources tend to be more variable at higher frequencies, the lack of a stronger correlation between the S/X spectral indices and the structure function slopes at 8.3 GHz is puzzling.

Figure 5 also shows that we are in general agreement with Paper I regarding the distribution of scattering toward these sources. At low latitudes, the logarithmic slope increases toward unity, as expected if scattering is better described as by volume than a single screen. The large scatter at low latitudes is due probably to the inhomogeneous distribution of scattering. Our lower value for the average logarithmic slope can be attributed to the larger number of high latitude sources for which scattering is likely to be less important.

3.4. Wavelet Transform Identification of Extreme Scattering Events

One of the primary motivations for conducting this series of observations was to identify additional extreme scattering events (Fiedler et al. 1987a). Extreme scattering events identified thus far from this data set are shown in Fiedler et al. (1994) and Clegg, Fey, & Lazio (1998). However, all previous ESEs have been identified visually. Here we attempt a systematic search for ESEs using a wavelet transform. Because of the strong wavelength dependence of ESEs, we focus on the 2.25 GHz light curves for this analysis.

A wavelet transform of a discretely sampled time series $F(t_i)$ is (e.g., Scargle 1989)

$$W_F(s,l) = \sum_i \psi(s,l;t_i)F(t_i). \tag{11}$$

The wavelet transform kernel $\psi(s,l)$ depends upon both a "scale" size s and a location l, in contrast to a Fourier transform kernel which depends upon only the frequency or scale size. As a consequence, wavelet transforms are useful in detecting features that are localized in time, including transient events.

In order to account for gaps in the time series, we followed a procedure suggested by Scargle (1989) for the autocorrelation function of a time series with missing data. We calculated $W_F(s,l)$ and $W_U(s,l)$, where $U(t_i)$ is a time series with the same sampling as $F(t_i)$ but with unit flux density. The analyzed quantity was (W_F/W_U). The wavelet coefficients W_U account for the uneven sampling of the time series; forming the ratio decreases the magnitude of coefficients W_F which occur largely because of the uneven sampling.

For the purposes of identifying ESEs, we compared two different wavelet kernels—the Haar and the mexican hat (Marr) bases. The former is a unit increase followed by a unit decrease and resembles the ingress (or the negative of the egress) of a (symmetric) ESE. The latter is the second derivative of a gaussian and closely resembles the negative of a (symmetric) ESE. We found that the mexican hat basis produced a larger response to ESEs already identified, and we shall use it in our analysis.

The wavelet coefficients themselves are the sum of a number of flux densities. The individual flux density measurements are nearly gaussian distributed (Paper I), and, by the central limit theorem, their sum will be even more nearly gaussian distributed. We exploit the gaussian distribution of the wavelet coefficients to search for ESEs in the following manner: For each scale s we have determined the mean and variance, σ_W^2, averaged over all locations l. Wavelet coefficients having less than a 99% probability of occurring by chance, i.e., those that deviate by more than $2.57\sigma_W$ from the mean, were considered to be potential ESEs.

The known ESEs have durations of roughly a few weeks to a few months. This typical duration is almost certainly a selection effect, as the shortest ESE that can be identified depends upon the sampling frequency and the longest ESE depends upon the duration of the light curve. With our typical sampling of one flux density measurement every two days, we will be unable to identify reliably ESEs with a duration of 8 days or less. For this reason we both smoothed the light curves by an 8-day boxcar (this also reduces the effects of the day-to-day variability) and considered only wavelet coefficients for scales 16 days or longer. The maximum duration of an ESE that we could detect is limited by the length of the monitoring program. Our ESE detection procedure also requires that there be a reasonable number of wavelet coefficients to form the mean and variance. For sources observed during 1988–1994, we restricted the largest scale to be $s \leq 128$ days; for the sources whose observations commenced prior to 1988, we allowed $s \leq 1024$ days.

The wavelet coefficients identified from this procedure as being significant comprise a set of candidate ESEs. However, instrumental changes or malfunctions could also result in a significant wavelet coefficient. In many cases, significant wavelet coefficients were found on the same or adjoining days for sources separated by tens of degrees on the sky. If two or more sources showed significant wavelet coefficients occurring within 4 days (i.e., 2 samples) of each other, we eliminated these wavelet coefficients from the set of candidate ESEs. Because an outburst from a source could also produce a significant coefficient, we examined visually the light curves in the vicinity of the significant coefficients. We eliminated wavelet coefficients that did not show a decrease in flux density, as would be expected from an ESE.

Table 5 lists the location of probable ESEs that survived this culling. Figure 7 shows the light curves in the vicinity of these ESEs.

Table 5. Wavelet-Identified ESEs in the GBI Monitoring Program

Name	Epoch	Significance (σ_W)
0133+476	1990.2	8.8
0201+113	1991.3	3.5
0202+319	1989.5	6.7
0300+470	1988.3	6.3
0528+134[a]	1991.0	2.9
	1993.9	9.6
0952+179[a]	1992.6	7.4
	1993.6	9.6
0954+658	1981.1	15.9
1438+385	1993.5	3.4
1502+106	1979.5	6.2
1756+237	1993.7	2.8
2251+244	1989.9	3.4
2352+495	1984.6	3.6

[a]Multiple ESEs were identified for this source.

Note. — Column (3), Significance, shows the number of standard deviations that the wavelet coefficient exceeds the mean.

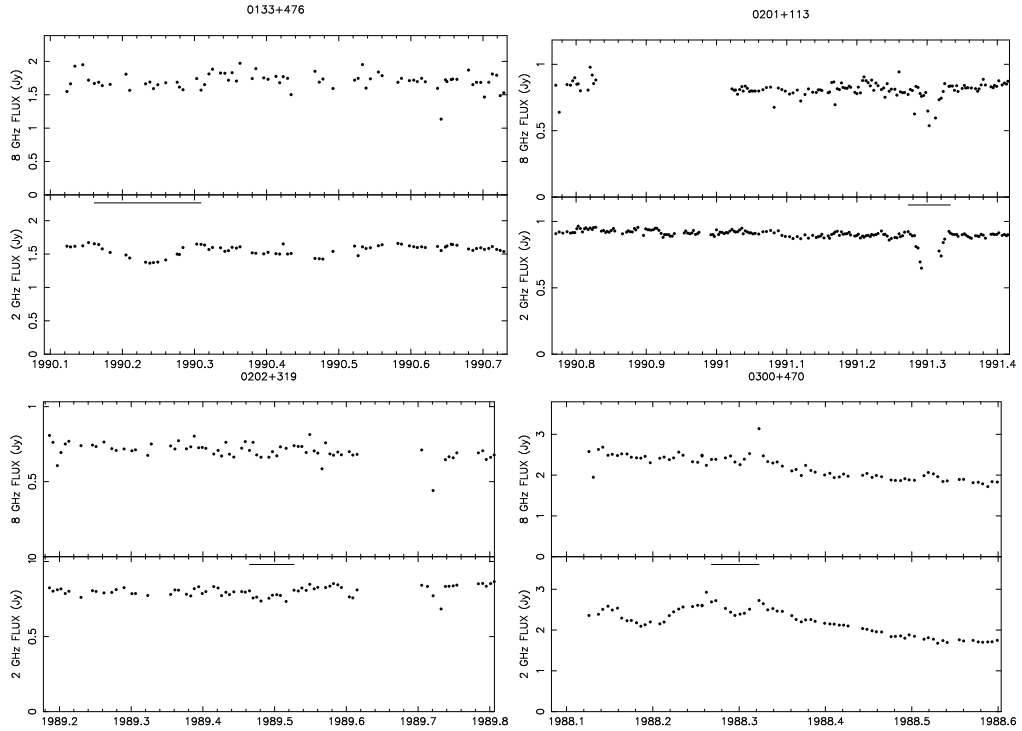

Fig. 7.— Light curves in the vicinity of probable extreme scattering events identified from the wavelet analysis. A horizontal bar near the top of the lower panel indicates the approximate duration of the ESE.

In a limited number of instances, significant wavelet coefficients occurred at times where multiple processes may have been occurring simultaneously. For instance, between 1985 and 1987 the source 1502+106 underwent an outburst (Figure 8). During the outburst both the 2.7 and 8.1 GHz flux densities show variations on shorter time scales. This short time scale variability may be the result of intrinsic variations of a newly ejected component, scintillation of a compact component produced in the outburst (Rickett 2000), and/or an ESE (Fiedler et al. 1994).

Having scanned the light curves in a systematic manner for ESEs, we can also address how many ESEs identified previously (Fiedler et al. 1992, 1994; Pohl et al. 1995) can be considered significant. Table 6 lists ESEs identified previously from the sources included in this monitoring program. Of the 12 ESEs identified previously, a substantial duration of the ESE for four sources (0133+476, 0300+471, 0528+134, 1749+096) occurred during a transition in the monitoring program. Although the effect of these ESEs can be seen in the GBI light curves, the identification of these ESEs is almost certainly due to monitoring programs being conducted simultaneously at other telescopes. Thus, their absence in our list of wavelet-identified ESEs is not surprising. As discussed above, the variability identified in the light curve of 1502+106 may not be due to an ESE.

Of the remaining 7 previously identified ESEs, only the ESEs toward 0954+658 and 2352+495 produce significant wavelet coefficients. Sources without significant wavelet coefficients at the time of a visually-identified ESE are 0333+321 (2 ESEs identified), 1611+343, 1741−038, and 1821+107.

For these latter four sources, we have examined the wavelet coefficients in the neighborhood of their ESEs. We find that, with the exception of 1741−038, there were potentially significant wavelet coefficients

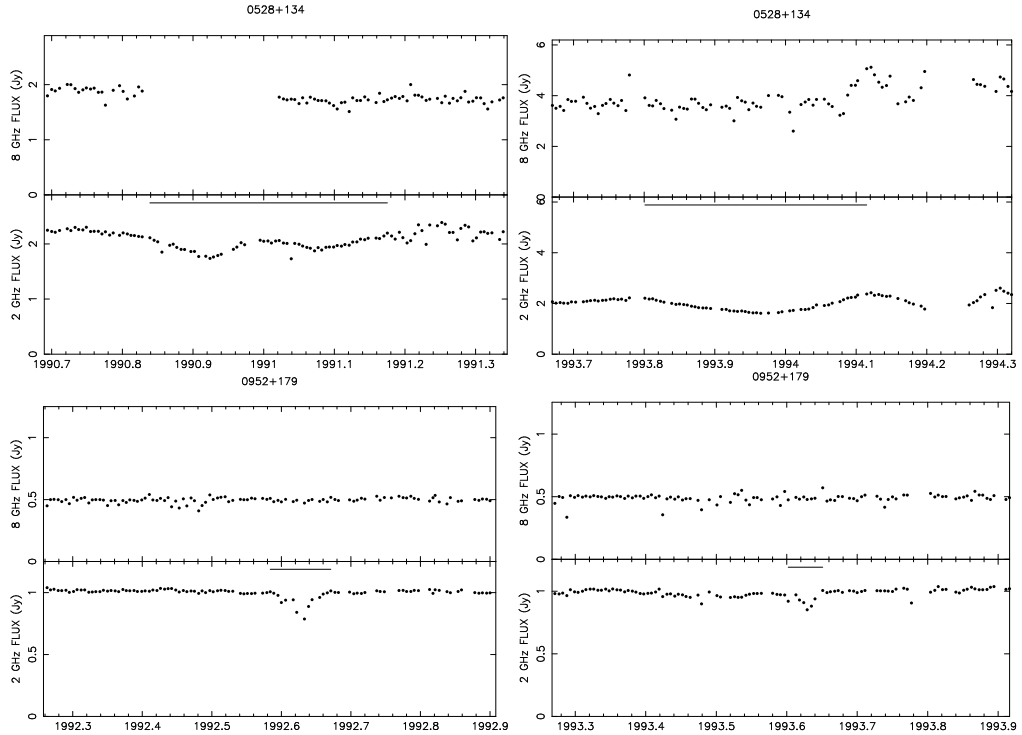

Fig. 7.— *Cont.*

that were culled by our requirement that there be no other sources having significant wavelet coefficients within 4 days.

In the presence of at least one instrumentally-induced variation, we regard this requirement as necessary. Nonetheless, we have re-examined the light curves for ESE-like features having potentially significant wavelet coefficients that were initially culled by this requirement. The epochs of these ESE-like features are listed in Table 7. We consider these ESE-like features as having an uncertain confidence level but include them here for completeness.

The light curve of 1741−038 shows considerable variation both before and after the ESE identified by Fiedler et al. (1992; cf. Figure 8). This source has been identified as showing considerable refractive scintillation (Hjellming & Narayan 1986; Dennison et al. 1987). Its light curve may be an indication that ESEs should indeed be considered not as distinct phenomenon, but as "extreme refractive events" (Rickett 1990) forming the extreme cases of variability due to refractive scintillation.

We consider it likely that future monitoring programs will need to continue relying on both systematic and visual identification of ESEs to separate instrumental and intrinsic variations of the sources.

4. Conclusions

We have presented multi-year radio light curves for a sample of 149 sources. The sources were monitored at two frequencies (approximately 2.5 and 8 GHz) for intervals ranging from 3 to 15 yr, with a monitoring frequency of roughly one flux density measurement every 2 days.

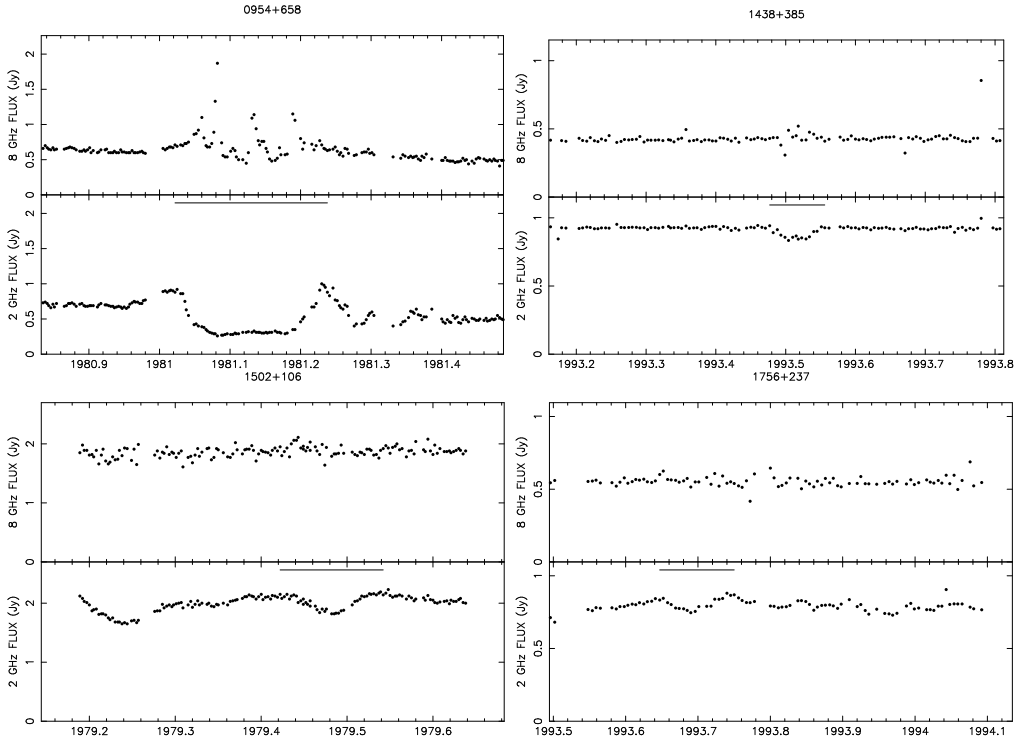

Fig. 7.— *Cont.*

We have used a variety of techniques to assess the variability of these light curves. The rms flux densities of the light curves are highly correlated between the two frequency bands. The variability is highly correlated with spectral index, with flat-spectrum sources more likely to be variable than steep-spectrum sources, and is more pronounced at the higher frequency, with a frequency scaling suggesting that the electron energy distribution in the flares has a power-law index of 2.5. We have also used low-order autoregressive, integrated, moving average models (ARIMA models) to characterize the light curves. We find that most sources can be described by a limited number of models. Further, we find that the same set of models describe sources at both frequencies. The combination of these two analyses suggests, though not entirely unambiguously, that these sources share a common, broadband emission mechanism.

A structure function analysis indicates the sources display a short-term ($\sim$ 10 d) variability due to radio-wave scattering. An earlier analysis on a subset of these sources found a logarithmic structure function slope of 1–1.5. We find a mean slope of 0.3 and a strong correlation of a source's structure function slope with its Galactic latitude, indicative of at least a fraction of our sources exhibiting radio-wave scattering through an extended medium. The lower mean slope in our larger sample as compared to that of Paper I may be indicative of the larger number of source at high latitudes for which scattering is likely to be less important.

The primary motivation for this monitoring program was the identification of extreme scattering events. In an effort to identify ESEs in a systematic manner, we have used a wavelet transform of the light curves to indicate intervals of significant variability. Distinguishing instrumentally-induced variations from ESEs is difficult for these data. Of 7 ESEs identified previously, only 2 were found to be significant in our wavelet analysis. Most of the remaining 5 ESEs produced a potentially large wavelet coefficient, but were at epochs

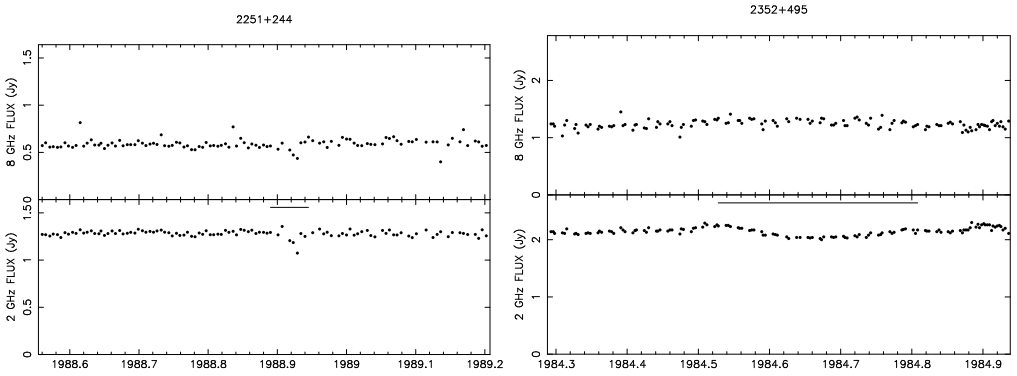

Fig. 7.— *Cont.*

when other sources did as well. Our wavelet analysis also found 15 events in the light curves of 12 sources that we consider to be probable ESEs. However, distinguishing ESEs in future monitoring programs will probably continue to require a combined approach of both systematic and visual inspections of light curves.

We believe that this sample of 149 sources, with light curves ranging from 6 to 15 yrs in length, presents a unique resource for studying both intrinsic and propagation-induced variability. The data presented here are available on the World Wide Web at the NRL GBI site, http://ese.nrl.navy.mil/.

We acknowledge the outstanding contribution of the staff of the Green Bank Interferometer in maintaining an aging, yet sensitive instrument. We thank P. Crane, A. Fey, and B. Rickett for helpful discussions and J. Imamura for assistance with Table 1. We thank the referee for helpful suggestions to improve the presentation of our results. This research made use of SIMBAD, at the CDS, Strasbourg, France, and the Astronomical Data System. A portion of this work was performed while TJWL held a National Research Council-NRL Research Associateship. The GBI is a facility of the National Science Foundation and was operated by the National Radio Astronomy Observatory under contract to the USNO and NRL during these observations. Basic research in radio astronomy at the NRL is supported by the Office of Naval Research.

REFERENCES

Aller, M. F., Aller, H. D., & Hughes, P. A. 1992, ApJ, 399, 16

Baars, J. W. M., Genzel, R., Pauliny-Toth, I. I. K., & Witzel, A. 1977, A&A, 61, 99

Blandford, R., Narayan, R., & Romani, R. W. 1986, ApJ, 301, L53

Bondi, M., Padrielli, L., Gregorini, L., Mantovani, F., Shapirovskaya, N., & Spangler, S. R. 1994, A&A, 287, 390

Box, G. E. P., Jenkins, G. M., Reinsel, G. C., & Jenkins, G. 1994 (Prentice Hall)

Charlot, P. 1990, AJ, 99, 1309

Clegg, A. W., Fey, A. L., & Lazio, T. J. W. 1998, ApJ, 496, 253

Coe, J. R. 1973, Proc. IEEE, 61, 1355

Condon, J. J., Condon, M. A., Broderick, J. J., & Davis, M. M. 1983, AJ, 88, 20

Dennison, B. et al. 1987, ApJ, 313, 141

de Vries, W. H., O'Dea, C. P., Barthel, P. D., & Thompson, D. J. 2000, A&AS, 143, 181

Drinkwater, M. J., et al. 1997, MNRAS, 284, 85

Fey, A. L. & Charlot, P. 2000, ApJS, 128, 17

Fey, A. L. & Charlot, P. 1997, ApJS, 111, 95

Fiedler, R. L., Dennison, B., Johnston, K. J., & Hewish, A. 1987a, Nature, 326, 675

Fiedler, R. L. et al. 1987b, ApJS, 65, 319 (Paper I)

Fiedler, R. L., Johnston, K. J., Waltman, E. B., & Ghigo, F. 1992, IAU Circ., 5527

Fiedler, R., Dennison, B., Johnston, K. J., Waltman, E. B., & Simon, R. S. 1994, ApJ, 430, 581

Foster, R. S., Waltman, E. B., Tavani, M., Harmon, B. A., Zhang, S. N., Paciesas, W. S., & Ghigo, F. D. 1996, ApJ, 467, L81

Ghosh, T. & Gopal-Krishna 1990, A&A, 230, 297

Hjellming, R. M. & Narayan, R. 1986, ApJ, 310, 768

Hewitt, A. & Burbidge, G. 1993, ApJS, 87, 451

Hewitt, A. & Burbidge, G. 1991, ApJS, 75, 297

Hogg, D. E., MacDonald, G. H., Conway, R. G., & Wade, C. M. 1969, AJ, 74, 1206

Hughes, P. A., Aller, H. D., & Aller, M. F. 1992, ApJ, 396, 469

Hughes, P. A., Aller, H. D., & Aller, M. F. 1991, ApJ, 374, 57

Hughes, P. A., Aller, H. D., & Aller, M. F. 1989b, ApJ, 341, 68

Hughes, P. A., Aller, H. D., & Aller, M. F. 1989a, ApJ, 341, 54

Kellermann, K. I. & Owen, F. N. 1988, in Galactic and Extragalactic Radio Astronomy, eds. G. L. Verschuur & K. I. Kellermann (Springer-Verlag: Berlin) p. 563

Koen, C. & Lombard, F. 1993, MNRAS, 263, 287

Marscher, A. P. & Gear, W. K. 1985, ApJ, 298, 114

McCollough, M. L., et al. 1999, ApJ, 517, 951

Ögelman, H. 1987, A&A, 172, 79

Pohl, M., et al. 1995, A&A, 303, 383

Pottschmidt, K., Koenig, M., Wilms, J., & Staubert, R. 1998, A&A, 334, 201

Ray, P., Foster, R. S., Waltman, E. B., Tavani, M., & Ghigo, F. D. 1997, ApJ, 491, 381

Rickett, B. J. 2000, in preparation

Rickett, B. J. 1990, ARA&A, 28, 561

Rickett, B. J., Coles, W. A., & Bourgois, G. 1984, A&A, 134, 390

Salgado, J. F., Altschuler, D. R., Ghosh, T., Dennison, B. K., Mitchell, K. J., & Payne, H. E. 1999, ApJS, 120, 77

Scargle, J. 1997, in Applications of Time Series Analysis in Astronomy and Meteorology, eds. T. S. Rao, M. B. Priestly, & O. Lessi (London: Chapman & Hall) p. 226

Scargle, J. 1990, ApJ, 359, 469

Scargle, J. 1989, ApJ, 343, 874

Scargle, J. 1981, ApJS, 45, 1

Simonetti, J. H., Cordes, J. M., & Heeschen, D. S. 1985, ApJ, 296, 46

Spinrad, H., Djorgovski, S., Marr, J., & Aguilar, L. 1985, PASP, 97, 932

Stickel, M. & Kühr, H. 1996, A&AS, 115, 1

Stickel, M. & Kühr, H. 1994, A&AS, 103, 349

Stickel, M., Meisenheimer, K., & Kühr, H. 1994, A&AS, 105, 211

Valtaoja, E., Terasranta, H., Urpo, S., Nesterov, N. S., Lainela, M., & Valtonen, M. 1992, A&A, 254, 80

Veron-Cetty, M. P. & Veron P. 2000, ESO Scientific Report, 19, 1

Waltman, E. B., Foster, R. S., Pooley, G. G., Fender, R. P., & Ghigo, F. D. 1996, AJ, 112, 2690

Waltman, E. B., Ghigo, F. D., Johnston, K. J., Foster, R. S., Fiedler, R. L., & Spencer, J. H. 1995, AJ, 110, 290

Waltman, E. B., Fiedler, R. L., Johnston, K. J. & Ghigo, F. D. 1994, AJ, 108, 179

Waltman, E. B., Fiedler, R. L., Johnston, K. J., Spencer, J. H., Florkowski, D. R., Josties, F. J., McCarthy, D. D., & Matsakis, D. N. 1991, ApJS, 77, 379

Zacharias, N., Zacharias, M. I., Hall, D. M., Johnston, K. J., de Vegt, C., & Winter, L. 1999, AJ, 118, 2511

Table 6. Previously Identified ESEs from the GBI Monitoring Program

Name	Epoch	Wavelet Identification?	Comments
0133+476	1988.2	no	occurred during GBI transition
0300+471	1988.2	no	occurred during GBI transition
0333+321[a]	1986.3	no	
	1987.9	no	
0528+134	1993.5	no	hardware malfunction, data lost
0954+658	1981.1	yes	
1502+106	1986.0	no	enhanced scintillation during outburst?
1611+343	1985.4	no	
1741−038	1992.5	no	
1749+096	1988.1	no	occurred during GBI transition
1821+107	1984.2	no	
2352+495	1985.0	yes	only partially identified

[a]Multiple ESEs were identified for this source.

Table 7. Potential ESEs in the GBI Monitoring Program

Name	Epoch
0003+380[a]	1990.3
	1992.2
0016+731	1992.5
0019+058	1991.2
0134+329	1988.9
0256+075	1991.6
0333+321	1988.6
0403−132	1993.0
0444+634	1992.0
0454+844	1993.4
0528+134[a]	1992.4
	1994.0
0555−132	1993.5
1438+385	1993.5
1502+106	1994.0
1538+149	1991.0
1614+051	1992.8
1635−035	1991.4
1741−038	1990.1
1821+107[a]	1991.0
	1993.6
2047+098	1993.0
2319+272	1992.5

[a]Multiple potential ESEs were identified for this source.

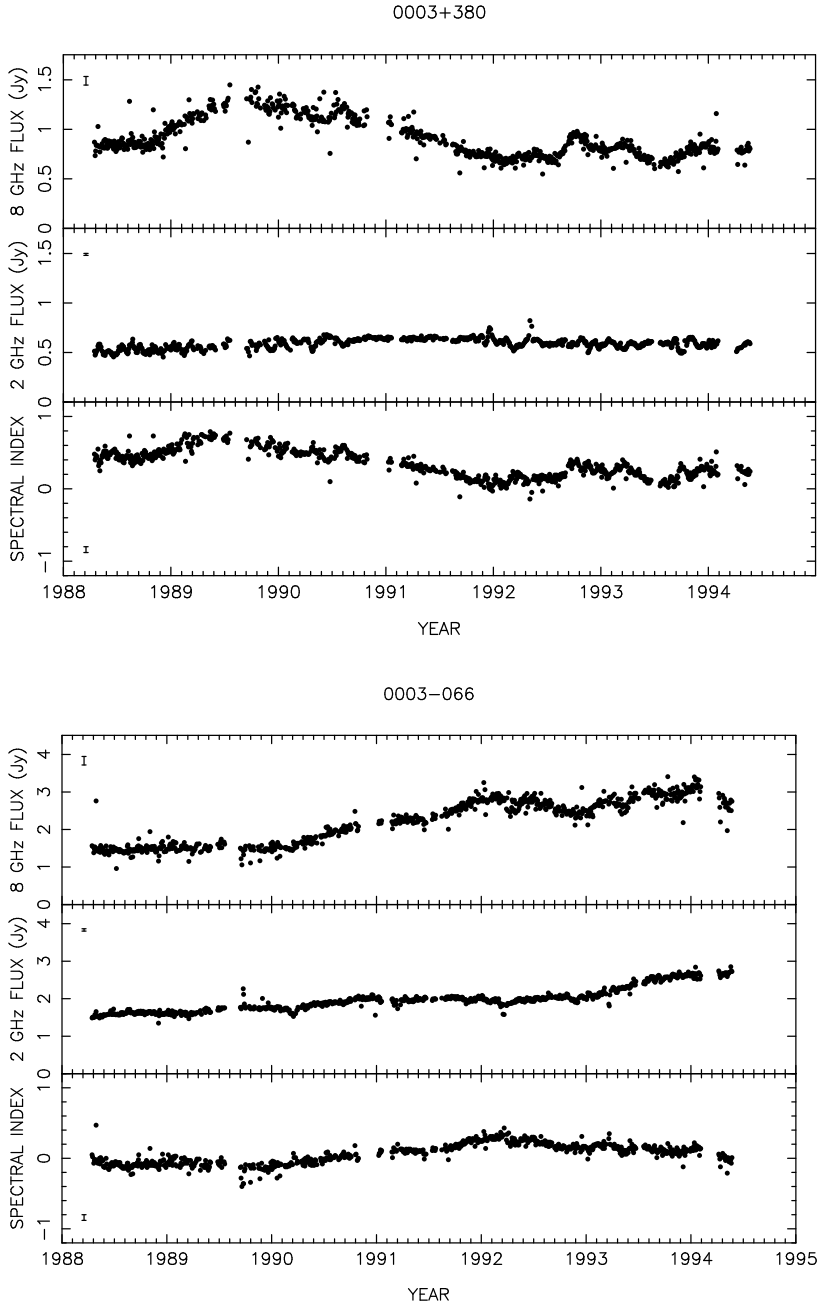

Fig. 8.— X-band (8 GHz) and S-band (2 GHz) light curves and S/X spectral indices. The discontinuities in flux levels at 1989.7 result from a change of observing frequency from 2.7 and 8.1 GHz to 2.25 and 8.3 GHz. The size of the typical measurement uncertainty is indicated at the left of each light curve. *Only a portion of Figure 8 is shown. All of Figure 8 and the data used to construct it are available at http://ese.nrl.navy.mil/GBI/GBI.html.*

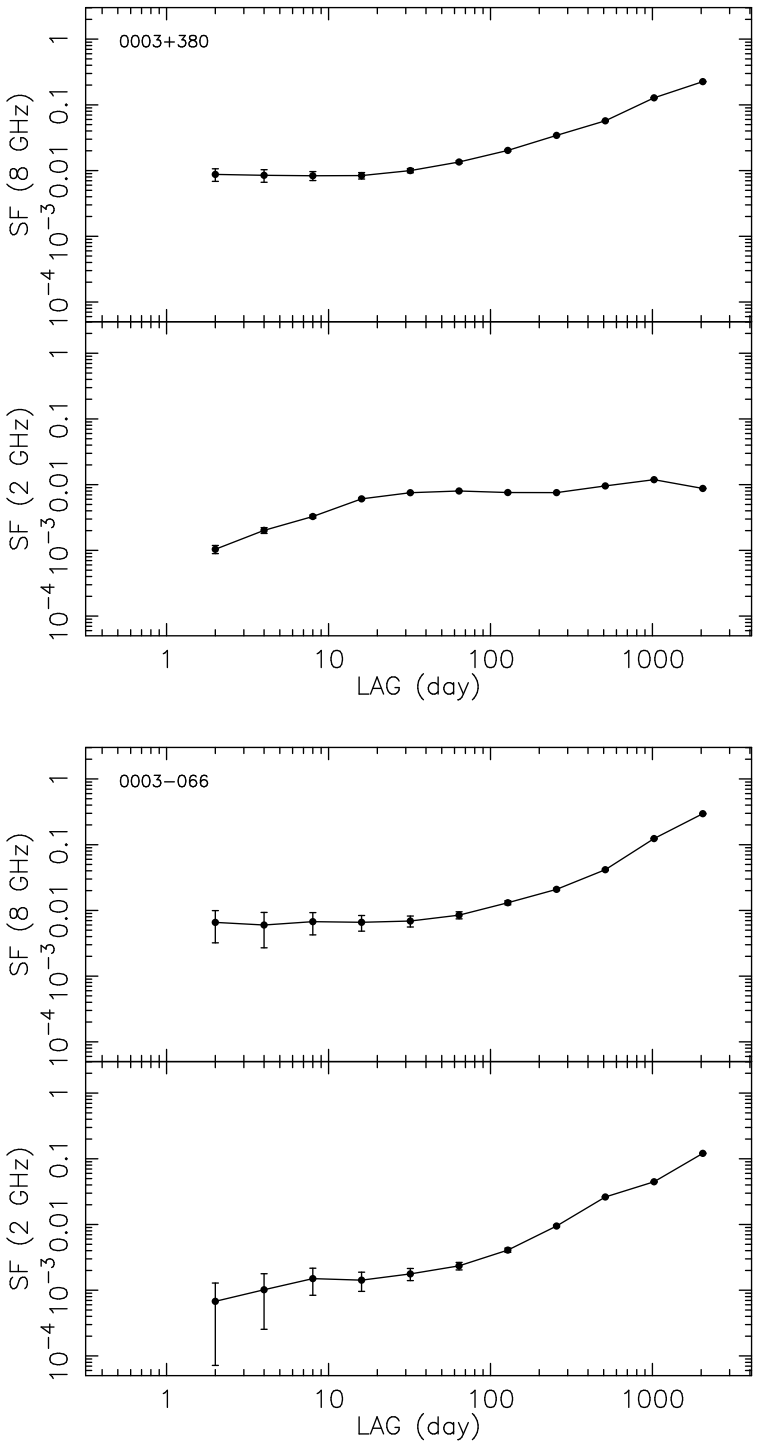

Fig. 9.— Structure functions. Structure functions were computed using equation (8), using *unsmoothed* light curves, and were normalized by the variance of the light curve. Pairs of data on opposite sides of the change in receivers (1989 August) do not contribute to these structure functions. *Only a portion of Figure 9 is shown. All of Figure 9 and the data used to construct it are available at http://ese.nrl.navy.mil/GBI/GBI.html.*